Data-Driven Robust Extended Computer Aided Harmonic Power Flow Analysis

O.S. Nduka and A.R. Ahmadi

July 14, 2020

Abstract

The surge in the uptake of harmonic producing loads in 21st century smart distribution networks has necessitated that robust data-driven approaches for harmonic assessment be developed. Moreover, there exists abundant harmonic data which can be leveraged on for the construction of this harmonic assessment tool. This is the objective of this paper. Large volumes of time-stamped data acquired from a practical distribution network in Edmonton, Canada, have been used to construct a time-dependent cross-coupled harmonic model that has been combined with a formulated iterative time-dependent robust extended computer-aided harmonic power flows. The constructed harmonic power flow formulation also considers the constraints relating to the power conservation principle at the fundamental frequency. Practical network conditions including untransposed lines, load unbalance and skin effects of conductors have been thoroughly modelled. The proposed method has been applied to practical radial and weakly-meshed medium voltage distribution networks and it demonstrated robustness to initialisation of the iterative procedure. Moreover, findings from this detailed data-driven technique reveal that harmonic impacts in the distribution networks depend on the quantum of harmonic levels, type of network and location of the harmonic sources.

Nomenclature

DG	Distributed generator
EMANA	Extended modified augmented nodal analysis
Superscripts r,i	Relates to real and imaginary parts of a term
Subscripts α, β	Used for arrays relating to real and imaginary term
m	m^{th} measurement
$\{k, h\}$	kth and hth harmonic orders
Subscript, n, ϕ	Relates to node 'n', phase ϕ
Subscript sl	Denotes slack bus term.
Subscript n, l	Denote n^{th} node and l^{th} line terms
h2	Second order harmonics
I^{inj}	Current injection
$I^{inj}_{n,\phi,k}$	k^{th} harmonic current of phase ϕ, node 'n'
I_{PQ} (I_G)	PQ load (Generator) current
J	Augmented vector of independent sources
MV, LV	Medium-, Low- voltage
$\hat{M}(W_\phi)$	Estimation model
NCE	Non-constitutive element
NLL	Nonlinear load
OLSE	Ordinary Least Squares Estimation
PCC	Point of common coupling
PFA	Power flow analysis
P,Q	Active and reactive powers
p_n	p^{th} NCE at the n^{th} node
RECAHPFA	Robust computer-aided harmonic PFA
RLSE	Recursive Least Squares Estimation
(t)	Time t
$V_{n,\phi}(t)$	Node 'n', phase-ϕ voltage at time t
U, T and D	NCE coefficient block matrices at h frequencies
$V_{n,\phi,1}$	h1 frequency voltage of phase ϕ, node 'n'
$y_{n,\phi_{21}}$	Admittance relating h1 voltage and h2 current
W_ϕ	Estimation parameters
ZIP	Impedance, current and power load
Θ^T_d	A regressor
$\left[\Omega\right]_i$	NCE current-related block matrix
$\left[\Omega\right]_v$	NCE voltage-related block matrix
$\left[\Psi\right]_z$	NCE impedance-related block matrix

1 Introduction

The high uptake of power electronic-based loads in electricity distribution systems has necessitated the development of harmonic assessment tools and their improved versions in recent times [1]-[6]. Some of the methods have been extended to study the network operating conditions in the presence of harmonic pollutions [7], [8].

Indeed, recent network planning and operational philosophy require that the 21^{st} century power distribution systems take into account the harmonic injection levels. This is relevant as more customer-owned power-electronic loads and interface units of distributed generators proliferate the distribution networks. For instance, [9]-[11] have reported that harmonic compliance requirements can limit the distributed generator (DG) hosting capacity in a practical power system. That is, a DG can be limited to supplying less than its available capacity in order to avoid violation of statutory harmonic limits. Similarly, issues relating to cable heating and ageing have also been reported [12]. These existing findings highlight the need for inclusion of harmonic assessment tools in the computational engine of modern distribution management systems. To this end, robust and accurate harmonic power flow tools capable of assessing practical network conditions while converging to a meaningful solution are highly desired.

Nevertheless, developing such computational tool is not trivial. This is because unlike conventional power flows, there are still open questions about the accuracy of certain representative models used in harmonic power flow formulation. Thus, solutions realised from some methods could be pessimistic whereas others are optimistic. Consider for instance the load models used for harmonic assessment - until now, there is no consensus on analytical load model (both linear and nonlinear types) for harmonic studies [13]. On the other hand, the accuracy of harmonic assessments is significantly influenced by the kind of load models adopted in the analysis [13], [14] .

To address the numerous challenges associated with the network component characteristics at harmonic frequencies, measurement-based approaches are gaining popularity among researchers in the power systems quality specialty. It is important to also state that some of the previously developed harmonic assessment methods have also relied on measurements. The differences lie in the volume of data and how the measurements were fitted into harmonic models. For instance, nonlinear load (NLL) models were classically modelled as constant current sources - ie. scaling the measured harmonic spectra with power level of the NLLs. However, existing research have proven that harmonic models that take into account the impact of the terminal voltages at the connection point offers more accurate description of the performance of the NLLs [1], [14].

For this voltage dependent harmonic current sources, decoupled and coupled harmonic models exist; with the latter been able to account for harmonic cross-couplings or interactions. The ability to capture such interactions between different harmonic frequency components is a desirable feature in any reliable harmonic assessment tool. The improvement in accuracy when coupled harmonic models are used is well-known [1], [2], [16].

Recently, [17] presented a practical method for the assessment of harmonics in the presence of limited data. The method investigated harmonic penetration in a medium voltage (MV) network with radial topology. The method essentially predicted harmonic current flows in a radial network with approximate and quick models and limited dataset. The authors however, confirmed that their proposed method could perform poorly where harmonic currents do not flow to the upstream power system.

As an alternative, the same paper (ie. [17]) reported a probabilistic approach which is essentially the classical Monte Carlo simulation technique. The harmonic load flow was solved for each harmonic order - i.e. a decoupled harmonic load flow. As the aim was for planning of an MV distribution network with limited dataset and using simple method, it made sense to neglect some complexities that exists in practical distribution networks such as phase imbalance and effects of untransposed lines. Nevertheless, as with advancements in classical power flows, harmonic power flow analysis still require methods that account for several network complexities and a unified approach that is network topology independent. Moreover, power conservation principle need to be included in any 'true' harmonic power flow method.

Beyond modelling complexities, another challenge with existing harmonic power flows is the initial iterates used in the simulation. That is, the initialization of a 3-phase harmonic power flow can be problematic especially if the initial variable estimates are not tuned close to values in the proximity of the solution [18], [19]. The likelihood of divergence increases if all the harmonic frequencies are solved at the same time with the unbalanced power flow constraints included in the formulation. It is obvious that the sophistication expands further where harmonic cross-couplings are modelled.

To avert the difficulties in convergence of iterative harmonic power flows, the traditional PQ constraints were relaxed in previous harmonic load flow analysis - i.e. PQ loads were transformed into constant admittances. Consequently, a non-iterative solution was adopted [18]. However, as loads in typical distribution networks could be a mixture of constant - power, admittance or current (ZIP power frequency loads) [20], the conversion of power loads to admittance loads at rated voltage and power levels could be misleading. Moreover, several representations of admittances exist for a constant power load [5], [13].

Harmonic power flows with the aim to overcome the described challenges have been attempted by other researchers. However, as noted in the literature, much attention has been devoted to the low voltage networks [8], [21], [22] and the transmission levels [4], [19], [23]. According to [21], only few studies have focussed on the MV level of distribution systems. For instance, [7] and [24] assessed MV distribution network performance in the presence of nonsinusoidal voltages and currents using the harmonic domain analysis reference frame first proposed in [25], [26]. In [27], the harmonic impacts of compact fluorescent lamps on distribution circuits were assessed using the harmonic Norton approach. Similarly, [28] assessed the impacts of harmonics from electric vehicle chargers on the distribution network. Ref. [17] has also proposed a method to assess harmonics in a radial MV distribution network with limited measurement

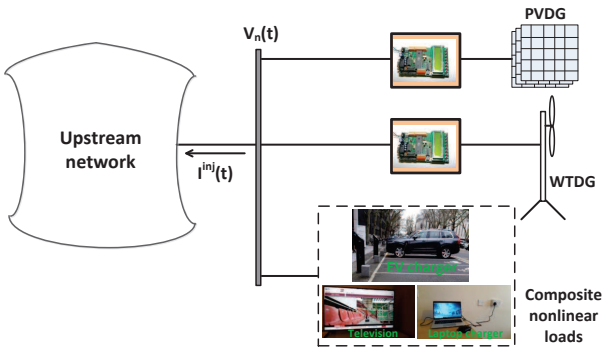

Figure 1: Illustrative diagram of composite harmonic generating sources

data.

Nevertheless, some of the aforementioned methods are either solely dedicated to the assessment of harmonic impacts of a cluster of a particular kind of NLLs or they are very computationally intensive technique with heavy modelling requirement for each harmonic producing load. Such cumbersome harmonic modelling may become impracticable in some instances - for example, consider the investigation of harmonic emissions from several wind turbines in a large wind farm. Fig. 1 shows an illustrative diagram of composite harmonic generating sources. Obviously, modelling each harmonic source separately and considering interactions with neighbouring harmonic sources for a system level study could pose a complicated problem.

Indeed, in the midst of simplistic as well as complex analytical techniques, abundant data now exist for several harmonic producing loads. Such data are yet to be fully mined. Moreover, [8], has demonstrated that although a particular harmonic producing device (or the cluster of the same devices) might not pose significant risk to the network, the interactions between several types of NLLs are worth investigating. Such interactions can only be fully captured through measurements at different operating instances of the nonlinear devices.

Consequently, this paper seeks to leverage on the available data for modelling of composite nonlinear loads and simultaneously deploying this load model in a robustly formulated computer aided harmonic power flow. The formulation handles the nonlinear constraints due to PQ loads and the slack bus at the power frequency while simultaneously considering the harmonically-coupled performance of the NLLs over an interval of timestamps. The method converges for both tuned (i.e. initalization with classical power flow results) and the 'flat start' iteration points. The flat start iterates involve using 1p.u voltage for the network nodes at power frequency and zero values for selected network component currents (called non-constitutive elements in the literature [29] both at fundamental and harmonic frequencies. Also, the harmonic voltages for all nodes are set to zeros. The proposed method deploys the Newton-Raphson technique and thus exhibits quadratic convergence.

Where the PQ constraints are relaxed, the method translates into a non-iterative technique which could be applied for real-time simulation. Due to the leveraging of data for the NLL modelling and the good numerical stability of the formulation (premised upon the enhanced modified augmented nodal analysis (EMANA) approach), the proposed computational tool is called data-driven robust extended computer-aided harmonic power flow (RECAHPFA) technique.

Summarily, the contributions of this paper are:

- A time-dependent data-driven harmonic power flow technique has been formulated.
- The proposed harmonic power flow method considered the modelling of a detailed 3-phase power distribution system - i.e. including untransposed lines, skin effects, and unbalance.
- The method included harmonic cross-couplings in the modelling evolution – i.e. the harmonic analysis formulation was conducted in an n-dimensional plane rather than the decoupled (2-dimensional) plane analysis.
- It fully accounted for power conservation (PQ) constraints without any relaxation assumptions.
- A method that is robust to initialization of state variables and agnostic to network topology (radial and weakly-meshed) has evolved from this research.
- The analyses have employed practical harmonic data with both magnitudes and phase angles – i.e. without any assumptions of phase angle diversities (cancellations and/or summations).
- The proposed method is a step forward in power quality data mining and leveraging of big data analytics for planning and operations of 21^{st} century power distribution networks.

In addition to the above introduction, other sections of the paper are arranged as stated next. In Section 2, the data-driven modelling approach for composite nonlinear loads is presented. Section 3 contains the evolution, construction and solution strategy for the proposed robust computer-aided harmonic power flow technique. While Sections 4 presents the experimental simulation of the method for a practical distribution network, Section 5 contains results and discussions. Furthermore, Section 6 compares the proposed method with existing harmonic power flow tools. Thereafter, is the conclusion to this technical work. There is also an Appendix section.

2 Data-driven nonlinear load model

Harmonic model construction from measurement data is well-known practice [1], [2]. Either the decoupled or coupled harmonic model is usually adopted

as highlighted previously. Such methods generally require measurement data at the point of common coupling (PCC) which are applied in constructing the equivalent combined admittance and current source model of the NLL. For this

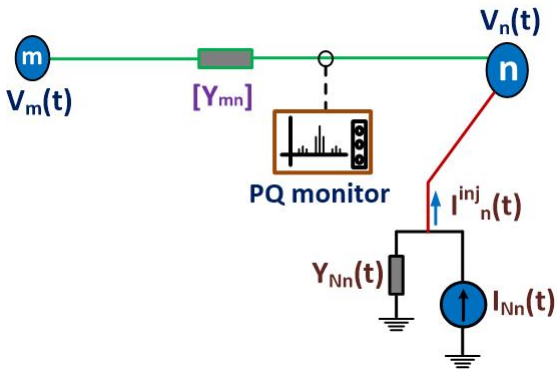

Figure 2: Illustrative diagram for constructing RLSE-based harmonic model

purpose, data acquired from field measurements by staff and partners of the Power Disturbance and Signalling laboratory of University of Alberta, Edmonton, Canada, have been used in this study. The coupled harmonic models have been constructed based on the Recursive Least-Squares Estimation (RLSE), essentially improving on the Ordinary Least Squares Estimation (OLSE) approach discussed in [1], [3]. For improved readability, a brief discussion on the OLSE as well as RLSE harmonic models and how the RLSE model was synchronised with the proposed harmonic assessment method is shown.

Consider the diagram in Fig. 2 which comprises a 2-node system with an NLL connected at node n; attention is devoted to this harmonics producing load. Based on physical (Kirchoff's current) law, the current injected into node 'n', $I^{inj}_{n,\phi}(t)$ can be mathematically described as (1).

$$I^{inj}_{n,\phi}(t) = I_{Nn}(t) - Y_{Nn}V_n(t) \tag{1}$$

For convenience, we considered per-phase load connected to each phase of the 3-phase system (i.e. grounded-wye loads) and thus ϕ denotes the phase. Considering also that node 'n' voltage, phase-ϕ, $V_{n,\phi}(t)$, comprises of a linear combination of different harmonic spectra, then, the expression (2), is valid for the

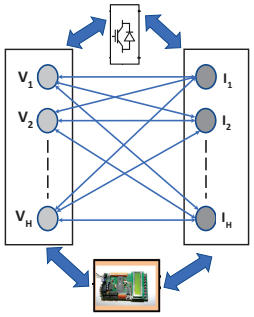

Figure 3: Illustration diagram of harmonic cross-coupling

harmonic domain expression.

$$I^{inj}_{n,\phi}(t) = \begin{bmatrix} I_{n,\phi,1}(t) \\ I_{n,\phi,2}(t) \\ \vdots \\ I_{n,\phi,H}(t) \end{bmatrix}_N - \begin{bmatrix} y_{n,\phi_{11}}(t) & y_{n,\phi_{12}}(t) & \dots & y_{n,\phi_{1H}}(t) \\ y_{n,\phi_{21}}(t) & y_{n,\phi_{22}}(t) & \dots & y_{n,\phi_{2H}}(t) \\ \vdots & \vdots & \dots & \vdots \\ y_{n,\phi_{H1}}(t) & y_{n,\phi_{H2}}(t) & \dots & y_{n,\phi_{HH}}(t) \end{bmatrix}_N \times \begin{vmatrix} V_{n,\phi,1}(t) \\ V_{n,\phi,2}(t) \\ \vdots \\ V_{n,\phi,H}(t) \end{vmatrix} \quad (2)$$

These harmonic interactions between the different harmonic spectra can be illustrated with the diagram in Fig. 3. Note that, as an example, $y_{n,\phi_{21}}(t)$ denotes the admittance that resulted from the contribution of the fundamental frequency voltage, $V_{n,\phi,1}(t)$, to the second order harmonic current of $I^{inj}_{n,\phi}(t)$, ie. $I^{inj}_{n,\phi,2}(t)$. Observe also, that the coupling admittance terms (e.g. $y_{n,\phi_{21}}(t)$) include the effect of the NLL power electronic components switching operation and the impacts of the operating conditions at the point of common coupling (PCC). The first vector in the right-hand side of (2) represents the harmonic current source.

As seen in the illustrative diagram (Fig. 3), the harmonic interactions depend on several factors including the type of NLLs, power converter control technology deployed in the devices, power levels, operating conditions at the point of interconnection etc. Thus, the harmonic cross-couplings are time-varying and also differs for different nonlinear devices. It is reasonable to conclude that the only realistic way to accurately capture these interactions is through field measurements and subsequent technical analysis of such data.

Indeed, the report by CIGRE [30, 31] clearly reveal that harmonic interactions - ('auto' and 'cross') sensitivities do exist. The field measurements [8] conducted by the same authors also confirms this.

From (2), it is possible to write each harmonic current injection in compact form as (3) and (4). Note that we have dropped the time-dependence from this

point in order to conserve space for the equations. We also dropped the node index 'n' for convenience.

$$I_{\phi,k}^{inj} = I_{N_{\phi,k}} - \sum_{h=1}^{H} y_{\phi,k,h} V_{\phi,h} \tag{3}$$

$$\Rightarrow I_{\phi,k}^{inj} = \begin{bmatrix} 1 & V_{\phi,1} & V_{\phi,2} & \dots V_{\phi,H} \end{bmatrix} \begin{vmatrix} I_{N_{\phi,k}} \\ -y_{\phi,k,1} \\ -y_{\phi,k,2} \\ \vdots \\ -y_{\phi,k,H} \end{vmatrix} \tag{4}$$

where in (3), $\{k, h\} \epsilon \{1, 2, 3, \dots, H\}$.

Given m-sets of measurements for each parameter in (4), the following expression ie. (5) is realised.

$$\begin{vmatrix} I_{\phi,k}^1 \\ I_{\phi,k}^2 \\ I_{\phi,k}^3 \\ \vdots \\ I_{\phi,k}^m \end{vmatrix} = \begin{bmatrix} 1 & V_{\phi,1}^1 & V_{\phi,2}^1 & \dots & V_{\phi,H}^1 \\ 1 & V_{\phi,1}^2 & V_{\phi,2}^2 & \dots & V_{\phi,H}^2 \\ 1 & V_{\phi,1}^3 & V_{\phi,2}^3 & \dots & V_{\phi,H}^3 \\ \vdots & \vdots & \vdots & \dots & \vdots \\ 1 & V_{\phi,1}^m & V_{\phi,2}^m & \dots & V_{\phi,H}^m \end{bmatrix} \begin{vmatrix} I_{N_{\phi,k}} \\ -y_{\phi,k,1} \\ -y_{\phi,k,2} \\ \vdots \\ -y_{\phi,k,H} \end{vmatrix} \tag{5}$$

The required parameters in (5) can be realised by solving an optimisation problem whose goal is to minimise the sum of squares of errors between the actual function and the estimate. We denote the estimation model as $\hat{M}(W_\phi)$ where:

$$\hat{M}(W_\phi) = \big[\Theta\big]\hat{W}_\phi \tag{6}$$

Then, the optimisation problem formulation is:

$$\underset{W_\phi}{\text{Min}} J_d(\hat{W}_\phi) = \sum_{d=1}^{m} \Big(\Gamma_d - \big[\Theta_d\big]\hat{W}_\phi\Big)^T \Big(\Gamma_d - \big[\Theta_d\big]\hat{W}_\phi\Big) \tag{7}$$

$$\rightarrow \underset{W_\phi}{\text{Min}} J(\hat{W}_\phi) = \Big(\Gamma - \big[\Theta\big]\hat{W}_\phi\Big)^T \Big(\Gamma - \big[\Theta\big]\hat{W}_\phi\Big) \tag{8}$$

The terms used in above expressions are defined as follows:

$$[\Theta] = \begin{bmatrix} 1 & V_{\phi,1}^1 & V_{\phi,2}^1 & \dots & V_{\phi,H}^1 \\ 1 & V_{\phi,1}^2 & V_{\phi,2}^2 & \dots & V_{\phi,H}^2 \\ 1 & V_{\phi,1}^3 & V_{\phi,2}^3 & \dots & V_{\phi,H}^3 \\ \vdots & \vdots & \vdots & \dots & \vdots \\ 1 & V_{\phi,1}^m & V_{\phi,2}^m & \dots & V_{\phi,H}^m \end{bmatrix}; \quad \Gamma = \begin{vmatrix} I_{\phi,k}^1 \\ I_{\phi,k}^2 \\ I_{\phi,k}^3 \\ \vdots \\ I_{\phi,k}^m \end{vmatrix} \tag{9}$$

$$\hat{W}_\phi = \begin{bmatrix} I_{N_{\phi,k}} & -y_{\phi,k,1} & -y_{\phi,k,2} & \dots & -y_{\phi,k,H} \end{bmatrix}^T \tag{10}$$

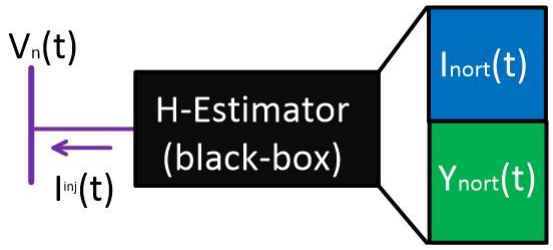

Figure 4: Schematic diagram of harmonic estimation

Θ_d^T denotes a regressor. Note also that the superscripts in (5) and (9) represent the measurement indexes. Superscript, T, denotes transpose.

Applying the condition of optimality by equating the derivative to zero and solving for the estimated parameters yields the solution in (11). This is the well-known OLSE method and it has been applied in [1] and [2], for estimating the harmonics from classical nonlinear devices.

$$\hat{W}_\phi = \Big([\Theta]^T[\Theta]\Big)^{-1}\Big([\Theta]^T\Gamma\Big) \tag{11}$$

The above equations are generally computed for each value of harmonic order of interest and then re-arranged to realise the current source and the cross-coupled harmonic admittance in (2). This technique can be diagrammatically represented as Fig. 4.

In this paper, the RLSE method has rather been applied. To use this method, the expression in (3) was written in the real-domain as shown in (12) and (13).

$$I_{\phi,k}^{inj,r} = I_{N_{\phi,k}}^{r} - \sum_{h=1}^{H}\Big(y_{\phi,k,h}^{r}V_{\phi,h}^{r} - y_{\phi,k,h}^{i}V_{\phi,h}^{i}\Big) \tag{12}$$

$$I_{\phi,k}^{inj,i} = I_{N_{\phi,k}}^{i} - \sum_{h=1}^{H}\Big(y_{\phi,k,h}^{r}V_{\phi,h}^{i} + y_{\phi,k,h}^{i}V_{\phi,h}^{r}\Big) \tag{13}$$

Considering m-measurements, then, the above equations are constructed as:

$$\Gamma_r = \big[\Theta_\alpha\big]W_{\phi,\alpha} \tag{14}$$

$$\Gamma_i = \big[\Theta_\beta\big]W_{\phi,\beta} \tag{15}$$

where:

$$\big[\Theta_\alpha\big] = \begin{bmatrix} 1 & -V_{\phi,1}^{r,1} & V_{\phi,2}^{i,1} & \dots & -V_{\phi,H}^{r,1} & V_{\phi,H}^{i,1} \\ 1 & -V_{\phi,1}^{r,2} & V_{\phi,2}^{i,2} & \dots & -V_{\phi,H}^{r,2} & V_{\phi,H}^{i,2} \\ 1 & -V_{\phi,3}^{r,1} & V_{\phi,2}^{i,3} & \dots & -V_{\phi,H}^{r,3} & V_{\phi,H}^{i,3} \\ \vdots & \vdots & \vdots & \dots & \vdots & \vdots \\ 1 & -V_{\phi,1}^{r,m} & V_{\phi,2}^{i,m} & \dots & -V_{\phi,H}^{r,m} & V_{\phi,H}^{i,m} \end{bmatrix} \tag{16}$$

$$\left[\Theta_{\beta}\right] = \begin{bmatrix} 1 & -V_{\phi,1}^{r,1} & -V_{\phi,2}^{i,1} & \dots & -V_{\phi,H}^{r,1} & -V_{\phi,H}^{i,1} \\ 1 & -V_{\phi,1}^{r,2} & -V_{\phi,2}^{i,2} & \dots & -V_{\phi,H}^{r,2} & -V_{\phi,H}^{i,2} \\ 1 & -V_{\phi,3}^{r,1} & -V_{\phi,2}^{i,3} & \dots & -V_{\phi,H}^{r,3} & -V_{\phi,H}^{i,3} \\ \vdots & \vdots & \vdots & \dots & \vdots & \vdots \\ 1 & -V_{\phi,1}^{r,m} & -V_{\phi,2}^{i,m} & \dots & -V_{\phi,H}^{r,m} & -V_{\phi,H}^{i,m} \end{bmatrix} \tag{17}$$

$$W_{\phi,\alpha} = \begin{bmatrix} I_{N_{\phi,k}}^{r} & y_{\phi,k,1}^{r} & y_{\phi,k,1}^{i} & \dots & y_{\phi,k,H}^{r} & y_{\phi,k,H}^{i} \end{bmatrix}^{T} \tag{18}$$

$$W_{\phi,\beta} = \begin{bmatrix} I_{N_{\phi,k}}^{i} & y_{\phi,k,1}^{r} & y_{\phi,k,1}^{i} & \dots & y_{\phi,k,H}^{r} & y_{\phi,k,H}^{i} \end{bmatrix}^{T} \tag{19}$$

The RLSE involves solving an optimisation problem similar to the OLSE [32]. Thus, we have:

$$\begin{aligned} \underset{W_{\phi,\alpha}}{\text{Min}} J(\hat{W}_{\phi,\alpha}) = \\ \sum_{x=0}^{m} \eta_r^{m-x} \left(\Gamma_{\alpha,x} - \left[\Theta_{\alpha,x}\right]\hat{W}_{\phi,\alpha}\right)^{T} \left(\Gamma_{\alpha,x} - \left[\Theta_{\alpha,x}\right]\hat{W}_{\phi,\alpha}\right) + \\ \eta_r^{m+1} \left(\hat{W}_{\phi,\alpha} - W_{\phi,\alpha,0}\right)^{T} \left[R_{\alpha}\right]^{-1} \left(\hat{W}_{\phi,\alpha} - W_{\phi,\alpha,0}\right) \end{aligned} \tag{20}$$

$$\begin{aligned} \underset{W_{\phi,\beta}}{\text{Min}} J(\hat{W}_{\phi,\beta}) = \\ \sum_{x=0}^{m} \eta_i^{m-x} \left(\Gamma_{\beta,x} - \left[\Theta_{\beta,x}\right]\hat{W}_{\phi,\beta}\right)^{T} \left(\Gamma_{\beta,x} - \left[\Theta_{\beta,x}\right]\hat{W}_{\phi,\beta}\right) + \\ \eta_i^{m+1} \left(\hat{W}_{\phi,\beta} - W_{\phi,\beta,0}\right)^{T} \left[R_{\beta}\right]^{-1} \left(\hat{W}_{\phi,\beta} - W_{\phi,\beta,0}\right) \end{aligned} \tag{21}$$

The solutions, $(\hat{W}_{\phi,\alpha})_{m+1}$, $(\hat{W}_{\phi,\beta})_{m+1}$, to the above optimisation problems can be derived similar to [32] viz:

$$\begin{aligned} \left[R_{\alpha}\right]_{m+1} = \frac{1}{\eta_r}\left[R_{\alpha}\right]_{m} - \frac{1}{\eta_r}\left[R_{\alpha}\right]_{m}\left[\Theta_{\alpha}\right]_{m}^{T} \Big(\eta_r^2[I] + \\ \left[\Theta_{\alpha}\right]_{m}\left[R_{\alpha}\right]_{m}\left[\Theta_{\alpha}\right]_{m}^{T}\Big)^{-1} \left[\Theta_{\alpha}\right]_{m}\left[R_{\alpha}\right]_{m} \end{aligned} \tag{22}$$

$$\begin{aligned} (\hat{W}_{\phi,\alpha})_{m+1} = (W_{\phi,\alpha})_{m} + \left[R_{\alpha}\right]_{m+1}\left[\Theta_{\alpha}\right]_{m+1}^{T} \times \\ \left(\Gamma_{m} - \left[\Theta_{\alpha}\right]_{m}(W_{\phi,\alpha})_{m}\right) \end{aligned} \tag{23}$$

$$\begin{aligned} \left[R_{\beta}\right]_{m+1} = \frac{1}{\eta_i}\left[R_{\beta}\right]_{m} - \frac{1}{\eta_i}\left[R_{\beta}\right]_{m}\left[\Theta_{\beta}\right]_{m}^{T} \Big(\eta_i^2[I] + \\ \left[\Theta_{\beta}\right]_{m}\left[R_{\beta}\right]_{m}\left[\Theta_{\beta}\right]_{m}^{T}\Big)^{-1} \left[\Theta_{\beta}\right]_{m}\left[R_{\beta}\right]_{m} \end{aligned} \tag{24}$$

Table 1: Calculated correlation coefficients

Harmonic order	Real component	Imaginary component
1	0.9993	0.9993
3	0.9962	0.9962
5	0.9971	0.9971
7	0.9957	0.9958

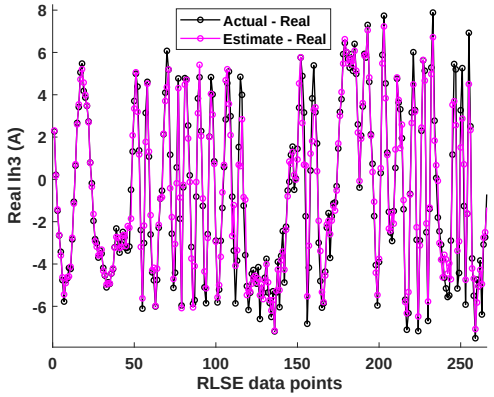

Figure 5: Plot of harmonic estimation: real part of h3 current

$$(\hat{W}_{\phi,\beta})_{m+1} = (W_{\phi,\beta})_m + \left[R_\beta\right]_{m+1}\left[\Theta_\beta\right]^T_{m+1}\times \left(\Gamma_m - \left[\Theta_\beta\right]_m (W_{\phi,\beta})_m\right) \tag{25}$$

Note that $\left[R_\alpha\right]_m \epsilon \mathbb{R}^{(1+2H)\times(1+2H)}$ and $\left[R_\beta\right]_m \epsilon \mathbb{R}^{(1+2H)\times(1+2H)}$ are positive definite terms and $\eta\epsilon(0,1]$. Also, $\left[\Theta_\beta\right]_m \epsilon \mathbb{R}^{m\times(1+2H)}$, $(\hat{W}_{\phi,\beta})_m \epsilon \mathbb{R}^{(1+2H)}$, $[I]\epsilon\mathbb{R}^{m\times m}$, $\Gamma_m \epsilon \mathbb{R}^m$ etc. Interested readers are encouraged to consult [32] for further insights into the RLSE approach.

2.1 Assessment of the RLSE technique

To validate the RLSE model with the measurement data, the correlation coefficient has been computed between the estimate and actual data. The closer this coefficient to unity, the better the performance of the estimator. For the first, third, fifth and seventh harmonic order, the following coefficients displayed in Table 1 have been realised. For completeness, the plots for the third and fifth harmonic orders are plotted as shown in Figs. (5), (6), (7), (8). Clearly, the estimation shows high accuracy.

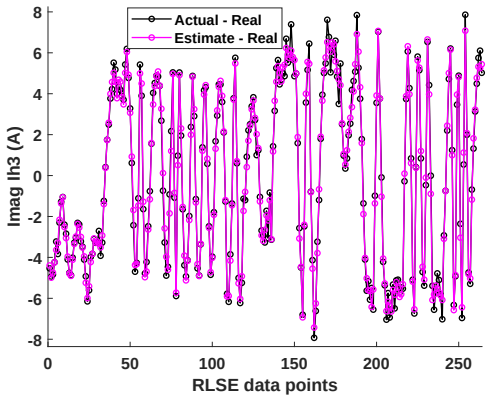

Figure 6: Plot of harmonic estimation: imaginary part of h3 current

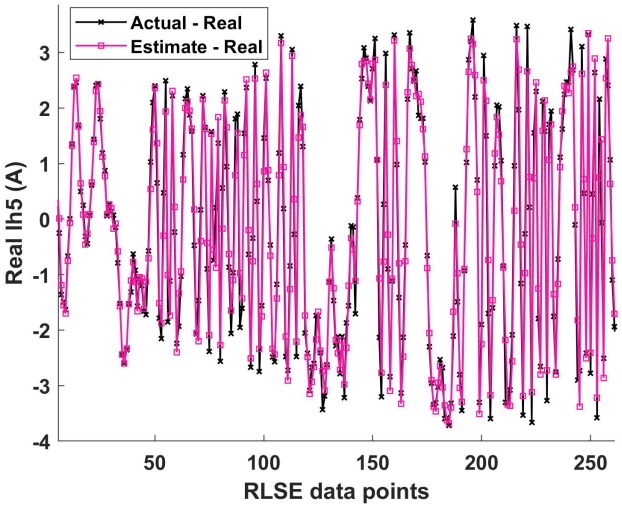

Figure 7: Plot of harmonic estimation: real part of h5 current

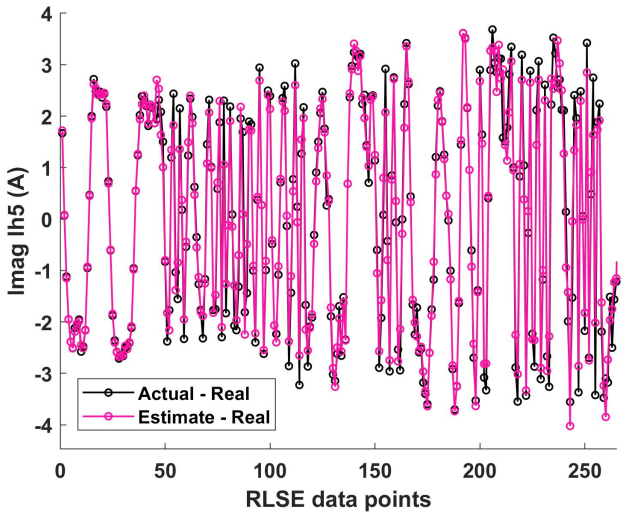

Figure 8: Plot of harmonic estimation: imaginary part of h5 current

3 Robust extended computer aided harmonic power flow analysis (RECAHPFA)

The RECAHPFA proposed in this paper leverages the strength of the EMANA technique previously developed by the same authors in [29]. The advantages of EMANA are mainly robustness and improved solvability. The RECAHPFA technique entails extending the EMANA to the harmonic frequencies while embedding the power frequency EMANA equations as equality constraints. Furthermore, the RLSE data-driven approach is integrated into the formulation for handling the harmonic-interactions of composite NLL models. The sections following, discuss the evolution of the construction of the RECAHPFA formulation and the solution strategy.

3.1 Equality constraint formulation

Based on the EMANA (see [29]), the fundamental frequency power flow are formulated as (26) and will appear as equality constraints in the proposed RECAHPFA as earlier outlined.

$$F_1^{(abc)}(X) = \left(\left[Y_{AugMat} \right] X_1 + I_{PQ} - I_G - J_1 \right)_1^{(abc)} = 0 \tag{26}$$

where:

$$\left[Y_{AugMat}\right] = \underset{\epsilon\mathbb{C}^{3(N+P_N)\times 3(N+P_N)}}{\begin{bmatrix} \left[Y_{(Stamp)}\right]^{(abc)} & \left[\Omega\right]_{i}^{(abc)} \\ \left[\Omega\right]_{v}^{(abc)} & \left[\Psi\right]_{z}^{(abc)} \end{bmatrix}} \tag{27}$$

$$X_1^{(abc)} = \begin{vmatrix} V_n^{(abc)} \\ I_{(p)_{sl}}^{(abc)} \\ I_{(p)_n}^{(abc)} \\ I_{(p)_l}^{(abc)} \end{vmatrix}; \quad V_n^{(abc)} = \begin{vmatrix} V_1^{(abc)} \\ V_2^{(abc)} \\ V_3^{(abc)} \\ \vdots \\ V_N^{(abc)} \end{vmatrix} \tag{28}$$

$$V_k^{(abc)} = \begin{bmatrix} V_k^{ax} & V_k^{bx} & V_k^{cx} & V_k^{ay} & V_k^{by} & V_k^{cy} \end{bmatrix}^T \tag{29}$$

$$I_{PQ}^{(abc)} = \begin{vmatrix} I_{(pq)_1}^{(abc)} \\ I_{(pq)_2}^{(abc)} \\ \vdots \\ I_{(pq)_N}^{(abc)} \\ O_{(3P_N\times 1)} \end{vmatrix}; I_G^{(abc)} = \begin{vmatrix} I_{(gen)_1}^{(abc)} \\ I_{(gen)_2}^{(abc)} \\ \vdots \\ I_{(gen)_N}^{(abc)} \\ O_{(3P_N\times 1)} \end{vmatrix} \tag{30}$$

$$\begin{aligned} I_{(s)}^{(abc)} &= \begin{bmatrix} I_{(p)_1}^{(abc)} & I_{(p)_2}^{(abc)} & \dots & I_{(p)_N}^{(abc)} \end{bmatrix}^T \\ V_{(s)}^{(abc)} &= \begin{bmatrix} V_{(p)_1}^{(abc)} & V_{(p)_2}^{(abc)} & \dots & V_{(p)_{P_N}}^{(abc)} \end{bmatrix}^T \end{aligned} \tag{31}$$

$$[Y_{stamp}]^{(abc)} = \underset{\epsilon\mathbb{C}^{3N\times 3N}}{\begin{bmatrix} \ddots & & & & \\ & [Y_{mm}]^{(abc)} & \dots & [Y_{mn}]^{(abc)} & \\ & \vdots & \vdots & \vdots & \\ & [Y_{nm}]^{(abc)} & \dots & [Y_{nn}]^{(abc)} & \\ & & & & \ddots \end{bmatrix}} \tag{32}$$

$$J_1 = \begin{vmatrix} I_{(s)}^{(abc)} \\ V_{(s)}^{(abc)} \end{vmatrix} \epsilon\mathbb{C}^{3(N+P_N)\times 1}; \quad X_1^{(abc)} = X_{h=1}^{(abc)} \tag{33}$$

It is important to note that all the equations presented herein are time-dependent but we have dropped the notation for convenience. In the equations above ((26) - (32)), I_{PQ}, I_G and J_1 respectively denote current due to PQ loads, generator current and augmented vector of independent current and voltage sources. The subscripts, sl, n and l implies terms relating to the slack bus, n^{th} node and l^{th} line. Similarly, the subscript, p_n, means the p^{th} non-constitutive element connected to the n^{th} node. $\left[\Omega\right]_i$, $\left[\Omega\right]_v$ and $\left[\Psi\right]_z$ are the

current, voltage and impedance coefficients (block matrices) obtained from the descriptive equations of the non-constitutive elements (see appendix section of [29] for examples). Note that non-constitutive components are elements whose currents are not purely expressible as functions of terminal voltages alone. Also, although the equations above appear in complex domain, they are transformed into the real-domain prior to deployment of Newton-Raphson which is presented later.

3.2 Harmonic analysis equation construction

For the harmonic frequencies ($h > 1$), we write

$$F_h^{abc}(X) = \left(\left[Y_{Hmat}\right] X - I_N - J_h \right)_{h=2:H}^{(abc)} = 0 \qquad \left[Y_{Hmat}\right] = \left[Y_{AugHmat} + Y_{AugNort}\right] \tag{34}$$

$$Y_{AugHmat} = \begin{bmatrix} [Y_{sth}] & [U]_{sl} & [U]_n & [U]_l \\ [T]_{sl} & [D]_{(zsl)} & & \\ [T]_n & & [D]_{(zn)} & \\ [T]_l & & & [D]_{(zl)} \end{bmatrix} \tag{35}$$

$$X^{(abc)} = \begin{vmatrix} X_1^{(abc)} \\ X_h^{(abc)} \end{vmatrix} \quad X_h^{(abc)} = \begin{vmatrix} X_2^{(abc)} \\ X_3^{(abc)} \\ \vdots \\ X_H^{(abc)} \end{vmatrix} \tag{36}$$

Note that the term $Y_{AugHmat}$ comprises elements of the line admittances (including the skin effects, series and shunt admittances) and capacitors. It has similar arrangement as (32) and hence we do not repeat the equation. Similarly, the harmonic admittance matrix $\left[Y_{AugNort}\right]$ has the form of (2) written for all nodes with nonlinear devices. The U, T and D terms are the appropriate coefficient block matrices for the non-constitutive elements at harmonic frequencies. The subscripts sl, n, and l are as defined previously. The above harmonic formulation is stacked up with the power flow constraints and solved iteratively.

To understand the above formulation, a conceptual diagram is provided in Fig. 9. We introduced a 'hypothetical switch' which is closed/triggered once there exists a harmonic order different from the fundamental ($h = 1$). The NLL harmonic model is constructed based on the RLSE applied to the measurement data as demonstrated previously. Combining the unbalanced 3-phase cross-coupled harmonic equations with the unbalanced 3-phase power flow constraints results in a set of equations that are highly nonlinear. This is especially due to the power flow constraints (especially PQ loads) and therefore, an iterative procedure is required. The Newton-Raphson method programmed using MATLAB have been used in this paper.

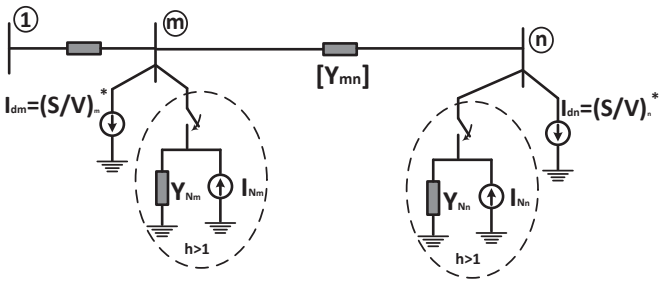

Figure 9: Conceptual diagram for the RECAHPFA

3.3 Solution Strategy

As previously mentioned, a data-driven harmonic Newton-Raphson approach has been applied to compute the solution variables of the above formulation. These variables include the node voltages at different harmonic frequencies as well as the currents of the non-constitutive elements at those frequencies. Note that variables for all frequencies are calculated at the same time unlike the decoupled harmonic load flows.

To apply Newton-Raphson technique, first, we linearized (26) and (34) as shown in (37).

$$\left[JAC^{abc}\right]^{(b)}\left(\triangle X^{abc}\right)^{(b)} = -\left(F_0^{abc}\right)^{(b)} \tag{37}$$

$$\left(X^{abc}\right)^{(b+1)} = \left(\triangle X^{abc}\right)^{(b)} + \left(X^{abc}\right)^{(b)} \tag{38}$$

where we have padded appropriately the linearized expressions as (39) and (40). Note that for an M-node system, with a slack bus, P_n non-constituent node elements and P_l total number of non-constituent line components, and with H harmonics of interest, the dimension of the Jacobian matrix is $\mathbb{R}^{6H(M+1+P_n+P_l)\times 6H(M+1+P_n+P_l)}$.

$$\left[JAC^{abc}\right]^{(b)} = \begin{bmatrix} \left[JAC^{abc}\right]_1^{(b)} \\ \left[JAC^{abc}\right]_h^{(b)} \end{bmatrix} \tag{39}$$

$$\left(F_0^{abc}\right)^{(b)} = \begin{bmatrix} \left(F_{0,h}^{abc}\right)^{(b)} \\ \left(F_{0,h}^{abc}\right)^{(b)} \end{bmatrix} \tag{40}$$

The Jacobian of the equality constraint has the form:

$$\left[JAC^{abc}\right]_1^{(b)} = \begin{bmatrix} [S] & [A]_{sl} & [A]_n & [A]_l \\ [B]_{sl} & [C]_{(zsl)} & & \\ [B]_n & & [C]_{(zn)} & \\ [B]_l & & & [C]_{(zl)} \end{bmatrix}_1 \tag{41}$$

To avoid repetitions for the 3-phase unbalanced power flow constraints and for the sake of space constraints, the authors recommend readers consult [29] for

the terms that appear in (41).

Similarly, the linearised version of the harmonic analysis equations are as shown in (42).

$$\begin{aligned}\left[JAC^{abc}\right]_h^{(b)} = \\ \begin{bmatrix} \left[Y_{Hmat}\right] & [U]_{sl} & [U]_n & [U]_l \\ [T]_{sl} & [D]_{(zsl)} & & \\ [T]_n & & [D]_{(zn)} & \\ [T]_l & & & [D]_{(zl)} \end{bmatrix} + \left[Y_{AugNort}\right]\end{aligned} \tag{42}$$

The right-hand side term in (37) is computed using the expressions (43) and (44).

$$F_h(X^{abc})^{(b)} = \left[\left(\left[Y_{Hmat}\right]X - I_N - J_h\right)_{h=2:H}^{(abc)}\right]^{(b)} \tag{43}$$

$$F_1(X^{abc})^{(b)} = \left[\left(\left[Y_{AugMat}\right]X_1 + I_{PQ} - I_G - J_1\right)_1^{(abc)}\right]^{(b)} \tag{44}$$

The above matrices and vectors representing the linearised expressions are appropriately embedded into the Newton-Raphson expression of (37).

3.4 Implementation of algorithm

The constructed RECAHPFA tool have been implemented following the logical sequence outlined below.

1. Identify types of nodes present in test network e.g. slack or PQ node
2. Identify all 'constitutive elements' and 'non-constitutive' network components [29].
3. Extract data from repository and specify RLSE interval
4. For $k = 1 : Nit$ where Nit is the number of RLSE intervals (value depends on the amount of data analyzed)
   a.) Apply FFT and RLSE techniques to obtain harmonically-coupled admittances and currents for considered RLSE interval
   b.) Initialize state variable X, set Error $= 10^{-6}$ and MaxIter $= 30$
   c.) while Iter $\leq$ MaxIter and Max $(| \triangle X|) >$ Error
   d.) Construct (41), (42), (43) and (44)
   e.) Solve (37)
   f.) Update state variable X using (38)
   g.) End iteration
   h.) Check if converged or diverged
5. Continue the process until k=Nit or exit if divergence occurred in previous step

Note that the background harmonics upstream the network have been modelled as voltage and current harmonic sources in the calculations and this has been consistently applied for all test cases. An alternative approach would include first, computing a simple harmonic power flows to deduce harmonic voltages at the nodes and thereafter including these harmonic voltage values in the data-driven approach. The latter method has already been presented by the first author in [24, 33].

3.5 Initialization

It is obvious that the Newton-Rapshon iterative procedure requires initial iterates. In fact, the choice of initial estimates has been a challenge to previous methods especially for three-phase analysis as reported in [18]. That challenge is overcome in the robust method presented in this paper. We have adopted two starting points as highlighted previously and both converged; thus, clearly demonstrating the robustness of the proposed approach. The only observed difference between the two starting points is that the tuned starting estimates converged in fewer iterations than the flat start iterates. Put differently, the tuned iterate took generally half the number of the iterations taken for the flat start to converge. This faster iteration convergence however comes at the cost of the tuning and may not be an advantage over the flat start in the true sense. Generally, the tuned simulation converged after the third iteration.

4 Experimental simulation

The application of the RECAHPFA computational tool proposed in this paper has been demonstrated using a practical MV distribution network of British Columbia, Canada, provided in [34]. The original network has a normally-open switch (NOS) between nodes '8' and '9'. While the original radial system has been studied, we have also closed this switch in another simulation scenario. With the switch closed, a part of the test system was transformed to a weakly-meshed topology. The idea was to test if the RECAHPFA method also converges for a network that has a subsystem that is weakly meshed. This will help to illustrate the versatility of the proposed method in the context of network topological structure.

Furthermore, the test MV network has unbalanced loading and untransposed lines. It also has a 3-phase, 64kV/25kV delta/wye grounded transformer between nodes '1' and '2', and a 3-phase capacitor at node '6'. The system is as shown in Fig. 10. All information required for detailed modelling of the skin effect and cross-couplings of the untransposed lines have been obtained from [34] as well as manufacturers datasheet.

We have considered each load point to have a service transformer, 14.4kV/0.12kV, 37.5 kVA, as it is typical of Canadian networks. The reason for this added service transformer at each load node is to investigate how the harmonic currents flowing downstream the service transformer (LV side) impact the upstream net-

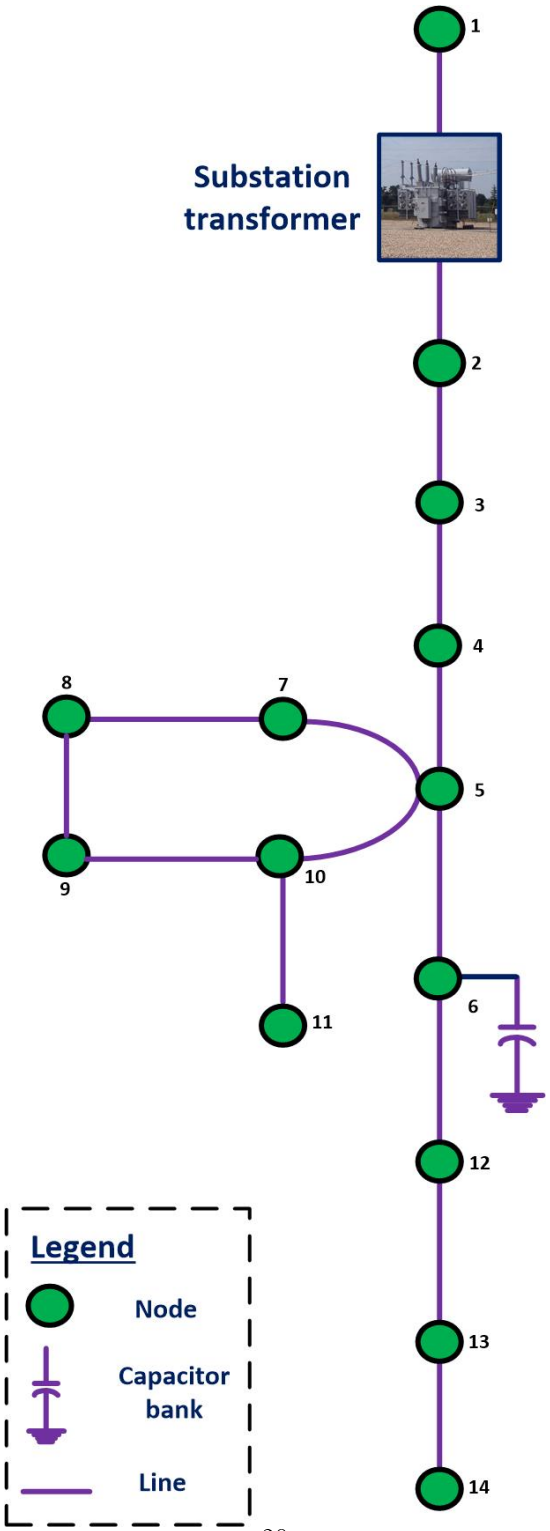

Figure 10: Test power network

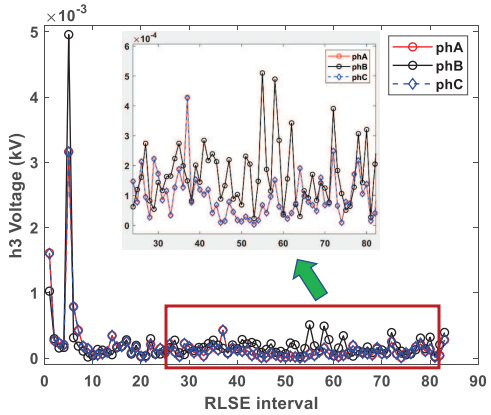

Figure 11: Radial: third harmonic voltage when PCC is at the LV side

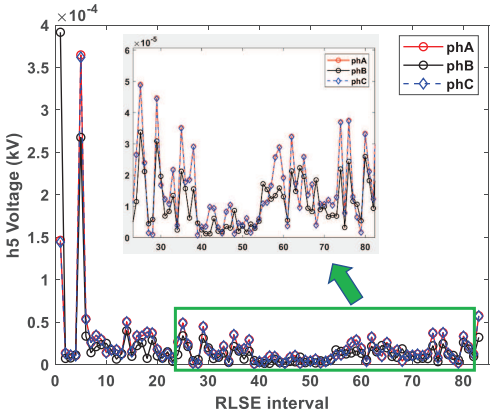

Figure 12: Radial: fifth harmonic voltage when PCC is at the LV side

work.

Indeed, this investigation of how harmonic sources at the LV levels of the distribution network influence the upstream network (MV level) is pertinent given that past research has made conclusions based on simplistic harmonic studies [1]. Thus, it became necessary to deploy this proposed method in analyzing time-varying harmonics in a practical distribution network.

For completeness, we also conducted the experimental simulation to assess the harmonic performance of the network should the harmonic sources be located at the HV-side of the MV network. Results of both cases are discussed as presented below.

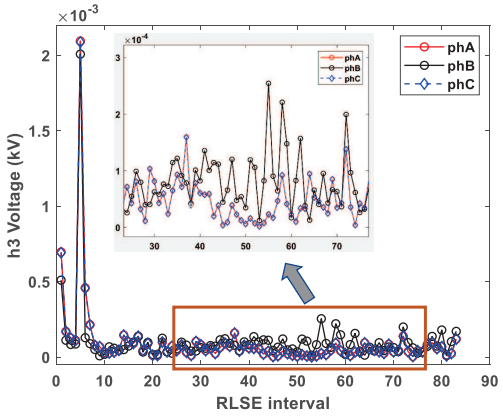

Figure 13: Meshed: third harmonic voltage when PCC is at the LV side

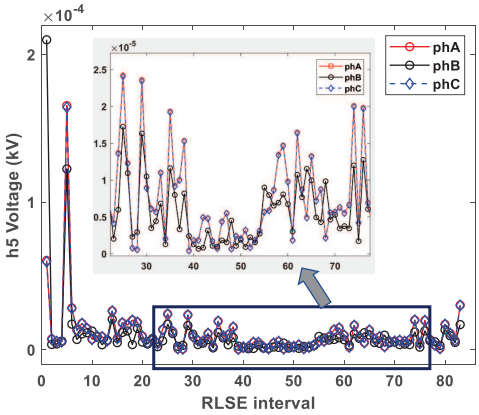

Figure 14: Meshed: fifth harmonic voltage when PCC is at the LV side

5 Results and discussions

Given the large amount of data for several days worth of data with time resolution in seconds (see Appendix for details), this paper only shows the simulation results for the RLSE intervals created from the evening peak hours (5:00pm - 7:10pm).

5.1 Assessing the harmonic levels when PCC for NLL is at the LV side

As mentioned previously, the first aspect of the simulation involved assessing the harmonic performance of the upstream system when the nonlinear devices were connected at the LV part of the distribution network. For space constraints,

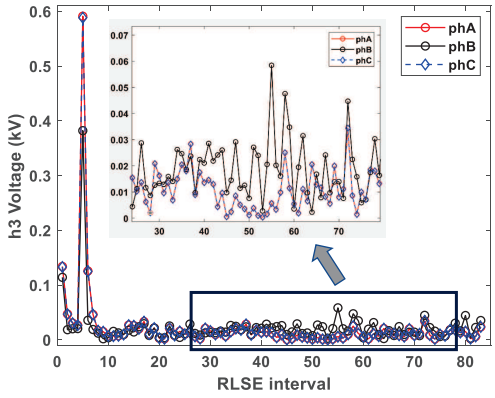

Figure 15: Radial: third harmonic voltage when PCC is at the HV side

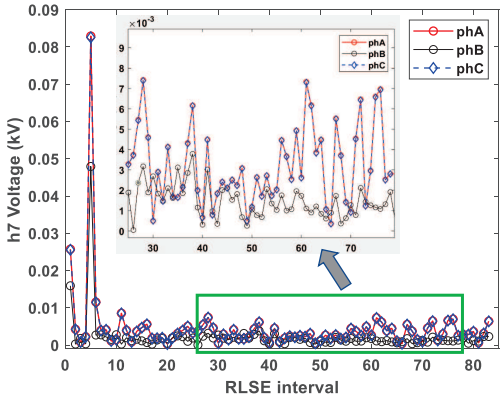

Figure 16: Radial: seventh harmonic voltage when PCC is at the HV side

only the third, fifth and seventh harmonic voltages of a particular node (node '9') are discussed. Fig 11 and Fig. 12 respectively show the plots for third and fifth harmonic voltages of this node for the test network with entirely radial configuration. Note that the voltages are expressed in kV.

Next, a portion of the network was re-arranged as a weakly-meshed configuration as described previously, the resulting third and fifth harmonic voltages at node 9 are as shown in Fig. 13 and Fig. 14.

Clearly, the harmonic voltages are negligible for both cases. This is not surprising given the impact of effective turns ratio of the service transformer which has further reduced the harmonic currents to very small values and thus they were unable to cause any significant harmonic voltage drop. Consequently, negligible distortion was noticed in the voltage waveform of node 9.

Based on this, it can be concluded that the residential harmonic loads at the LV side of the network do not pose a challenge to the upstream network in so

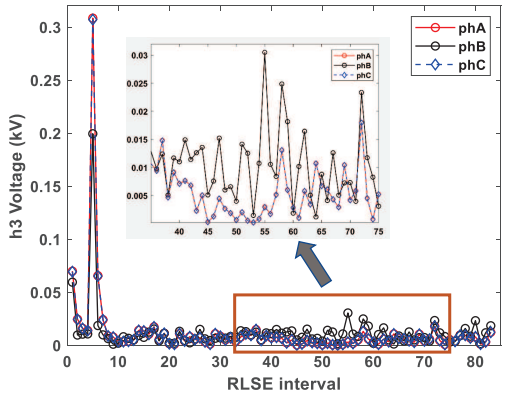

Figure 17: Meshed: third harmonic voltage when PCC is at the HV side

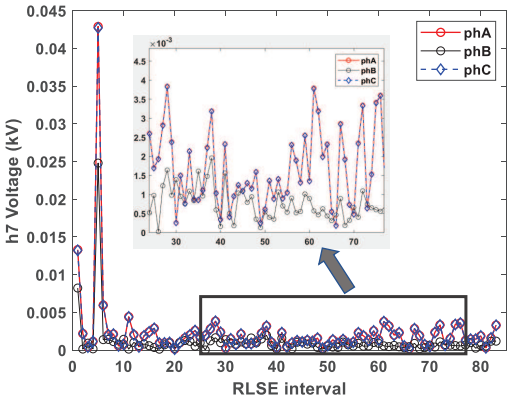

Figure 18: Meshed: seventh harmonic voltage when PCC is at the HV side

far as resonance excitation does not occur in the test system.

5.2 Harmonic levels when PCC is at the HV side of the MV network

For the purpose of completeness, the PCC is now considered as the HV side (ie. line-to-line voltage of 25kV) of the MV test network and simulation repeated both for the radial and meshed topologies. Indeed, this is likely the case due to a high demand customer, electric vehicle charging station or when a large DG (solar and/or wind farms) capacity form part of the system. Again we show the results for node 9 alone.

Fig. 15 and Fig. 16 are the third and seventh harmonic voltages for the radial configuration with the NLLs present at the HV-side of the MV network. Similar plots corresponding to when a portion of the system is weakly-meshed

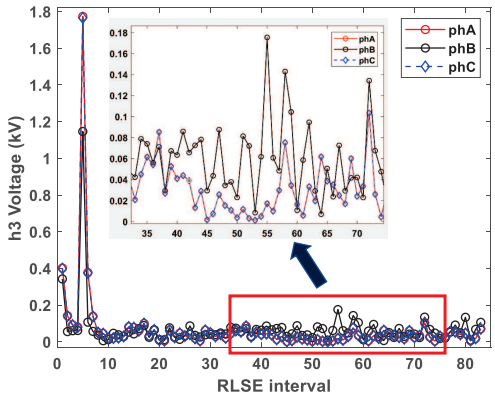

Figure 19: Illustration of impact of high harmonic current on harmonic voltage

are as shown in Fig. 17 and Fig. 18. Clearly, the harmonic voltages that appear at node 9 for both cases are now significant.

At this point, it is relevant to highlight that the total harmonic distortion of current at the point of maximum load is less than 9%. Should the current be higher, then higher harmonic voltages will appear across node 9 as shown in Fig. 19.

This confirms that the quantum of harmonic penetration in the network depends on the capacity of the harmonic generating sources and their locations in the network. Also, results for the radial and meshed systems are different generally. Hence generalisation of harmonic performance without taking into account these practical conditions would often result to either optimistic or pessimistic results.

6 Comparison of methods

As previously highlighted, there exists other harmonic power flow analysis techniques in the literature. However, the method we have presented in this paper is a datacentric approach that includes both practical network operating conditions and power conservation constraints. Such constraints were ignored by previous works which have replaced loads as admittance elements. A summary of the differences between the proposed method (denoted as 'P-method' in the table) and other harmonic power flow studies are as provided in Table 2.

Furthermore, a simulation for a simple case using the classical current source model yields equivalent voltage total harmonic distortion of 0.070. See IEEE recommendations [35, 36], and also as provided in Appendix, how equivalent voltage total harmonic distortion (THD) is calculated. For the same interval of consideration, the equivalent voltage THD of the proposed method yielded 0.0324. This suggests that simple current source representation of harmonics

Table 2: Summary of comparison of different harmonic power flow techniques

Indicator	[4]	[27]	[18, 23]	P-method
PQ-constraints	No	No	No	Yes
Harmonics Coupling	Yes	No	No	Yes
Data-intensive framework	No	No	No	Yes
Time-varying harmonics	No	No	No	Yes
Unbalanced consideration	Yes	No	Yes	Yes

from nonlinear loads can sometimes lead to pessimistic harmonic levels. Similar conclusions about the use of simple current models were observed in [1].

7 Conclusion

In this paper, a data-driven robust extended computer-aided harmonic power flow analysis tool has been developed. Data has been obtained from field trials of a practical distribution network in Canada. The method discussed overcomes the need for complex modelling of each harmonic source which becomes impracticable when several harmonic sources exist in the system. On the other hand, it involves more detailed and accurate modelling than the simple approaches that exist in current literature. The proposed tool has been applied in the study of practical MV networks while taking into account the time-varying nature of the harmonic loads and practical complex distribution network operating conditions such as skin effect, load unbalance and untransposed lines. Both radial and weakly-meshed configured networks have been studied. The method has demonstrated robustness as both tuned and 'flat' start initialisation points converged. It has also been established that harmonic performance for radial and meshed distribution networks are not necessarily the same and thus generalisation should be limited.

Acknowledgment

The authors would like to express their gratitudes to Prof. B.C. Pal of Imperial College and Prof. W. Xu of the University of Alberta, Canada, for very useful discussions. Moreover, Prof Xu provided the authors with field measurement data used for this study. We are also grateful to the reviewers for their useful feedback.

The first (corresponding) author is also thankful for the financial support received from the Joint UK-India Clean Energy (JUICE) Centre for this research. He (first/lead author) was involved in this research while he was at Imperial College London as a Postdoctoral Research Associate but he has recently moved to Royal Holloway University of London as a Lecturer (Assistant Professor) in Power Sustainability.

References

[1] C.F.M Almeida and N. Kagan, 'Harmonic coupled Norton equivalent model for modeling harmonic-producing loads', Proceedings of 14th International Conference on Harmonics and Quality of Power-ICHQP, IEEE 2010, pp. 1-9, 2010

[2] A.B. Nassif, J. Yong, W. Xu, 'Measurement-based approach for constructing harmonic models of electronic home appliances', IET generation, transmission & distribution, vol. 4, no. 3, pp. 363-75, Mar 1, 2010.

[3] A.S. Koch, J.M. Myrzik, T. Wiesner, L. Jendernalik, 'Evaluation and validation of Norton approaches for nonlinear harmonic models' In 2013 IEEE Grenoble Conference, pp. 1-6, June 16, 2013.

[4] T. Noda, A. Semlyen, R. Iravani, 'Entirely harmonic domain calculation of multiphase nonsinusoidal steady state', IEEE Transactions on Power Delivery, vol. 19, no. 3, pp. 1368-1377, Jun. 28, 2004.

[5] M. Madrigal and E. Acha, 'A new harmonic power flow method based on the instantaneous power balance' In 10th International Conference on Harmonics and Quality of Power. Proceedings (Cat. No. 02EX630), vol. 2, IEEE 2002, pp. 655-662.

[6] J.H. Teng and C.Y. Chang, 'Backward/forward sweep-based harmonic analysis method for distribution systems', IEEE Transactions on Power Delivery, vol. 22, no. 3, 1665-72, Jul 2, 2007.

[7] O.S. Nduka and B.C. Pal, 'Quantitative evaluation of actual loss reduction benefits of a renewable heavy DG distribution network', IEEE Transactions on Sustainable Energy, vol. 9, no. 3, pp. 1384-96, Dec 19, 2017.

[8] O.S. Nduka, L.P. Kunjumuhammed, B.C. Pal, A. Majumdar, Y. Yu, S. Maiti, A.R. Ahmadi, 'Field Trial of Coordinated Control of PV and Energy Storage Units and Analysis of Power Quality Measurements' IEEE Access, Dec 20, 2019.

[9] I.N. Santos, V. Ćuk, P.M. Almeida, M.H. Bollen, P.F. Ribeiro, 'Considerations on hosting capacity for harmonic distortions on transmission and distribution systems', Electric Power Systems Research, vol. 119, pp. 199-206, Feb 1, 2015.

[10] S. Sakar, M.E. Balci, S.H. Aleem, A.F. Zobaa, 'Hosting capacity assessment and improvement for photovoltaic-based distributed generation in distorted distribution networks', In 2016 IEEE 16th international conference on environment and electrical engineering (EEEIC), IEEE, pp. 1-6, Jun 7, 2016.

[11] S. Sakar, M.E. Balci, S.H. Aleem, A.F. Zobaa, 'Integration of large-scale PV plants in non-sinusoidal environments: Considerations on hosting capacity and harmonic distortion limits', Renewable and Sustainable Energy Reviews, VOL. 82, PP. 176-86, Feb 1, 2018.

[12] K.D. Patil, W.Z. Gandhare, 'Effects of harmonics in distribution systems on temperature rise and life of XLPE power cables', In 2011 International Conference on Power and Energy Systems, IEEE, pp. 1-6, Dec 22, 2011.

[13] CIGRE, 'C4/b4 technical brochure: Network modelling for harmonic studies,' 2019

[14] R. Burch, G.K. Chang, C. Hatziadoniu, M. Grady, Y. Liu, M. Marz, T. Ortmeyer , S. Ranade, P. Ribeiro, W. Xu, 'Impact of aggregate linear load modeling on harmonic analysis: A comparison of common practice and analytical models,' IEEE Transactions on Power Delivery, vol. 18, no. 2, pp. 625-30, Apr. 15, 2003.

[15] E. Thunberg and L. Soder, 'A Norton approach to distribution network modeling for harmonic studies,' IEEE Transactions on Power Delivery, vol. 14, no. 1, pp. 272-277, Jan. 1999.

[16] X. Xu, A.J. Collin, S.Z. Djokic, S. Müller, J. Meyer, R. Langella, A. Testa, 'Evaluation of hybrid harmonic modelling techniques: Case study of harmonic interactions of EVs and CFLs,' In 2016 IEEE PES Innovative Smart Grid Technologies Conference Europe (ISGT-Europe), IEEE, pp. 1-6, Oct 9, 2016.

[17] S. Abdelrahman and J.V. Milanović, 'Practical Approaches to Assessment of Harmonics Along Radial Distribution Feeders,' IEEE Transactions on Power Delivery, vol. 34, no. 3, pp. 1184-92, Feb 25, 2019.

[18] W. Xu and S.J. Ranade, 'Analysis of Unbalanced Harmonic Propagation in Multiphase Power Systems,' Tutorial on Harmonics Modelling and Simulation, 2004.

[19] G.N. Bathurst, B.C. Smith, N.R. Watson, J. Arillaga, 'A modular approach to the solution of the three-phase harmonic power-flow,' In 8th International Conference on Harmonics and Quality of Power. Proceedings (Cat. No. 98EX227), vol. 2, IEEE, pp. 653-659, Oct 14, 1998.

[20] K. Wang, H. Huang, C. Zang, 'Research on time-sharing ZIP load modeling based on linear BP network,' In 2013 5th International Conference on Intelligent Human-Machine Systems and Cybernetics, vol. 1, IEEE, pp. 37-41, Aug 26, 2013.

[21] Y. Wang, J. Yong, Y. Sun, W. Xu, D. Wong,' 'Characteristics of harmonic distortions in residential distribution systems,' IEEE Transactions on Power Delivery, vol. 32, no. 3, pp. 1495-504, Sep 8, 2016.

[22] J. Meyer, P. Schegner, K. Heidenreich, 'Harmonic summation effects of modern lamp technologies and small electronic household equipment,' In Proc. 21st International. Conf. on Electricity Distribution (CIRED), Jun 6, 2011.

[23] W. Xu, H.W. Dommel, J.R. Marti, 'A generalised three-phase power flow method for the initialisation of EMTP simulations,' In POWERCON'98. 1998 International Conference on Power System Technology. Proceedings (Cat. No. 98EX151), vol. 2, IEEE, pp. 875-879, Aug 18, 1998.

[24] O.S. Nduka and B.C. Pal, 'Harmonic domain modeling of PV system for the assessment of grid integration impact,' IEEE Transactions on Sustainable Energy, vol. 8, no. 3, 1154-65, Feb 3, 2017.

[25] J. Arrillaga, A. Medina, M.L. Lisboa, M.A. Cavia, P. Sanchez, 'The harmonic domain. A frame of reference for power system harmonic analysis,' IEEE Transactions on Power Systems, vol. 10, no. 1, pp. 433-440, Feb. 1995.

[26] J. Arrillaga and N.R. Watson, 'The harmonic domain revisited,' In 2008 13th International Conference on Harmonics and Quality of Power, IEEE, pp. 1-9, Oct. 2008.

[27] N.R. Watson, T.L. Scott, S.J. Hirsch, 'Implications for distribution networks of high penetration of compact fluorescent lamps,' IEEE transactions on power delivery, vol. 24, no. 3, pp. 1521-8, Mar 27, 2009.

[28] C. Jiang, R. Torquato, D. Salles, W. Xu, 'Method to assess the power-quality impact of plug-in electric vehicles,' IEEE Transactions on Power Delivery, vol. 29, no. 2, pp. 958-965, Oct 16, 2013.

[29] O.S. Nduka, Y. Yu, B.C. Pal, E.C. Okafor, 'A Robust Augmented Nodal Analysis Approach to Distribution Network Solution,' IEEE Transactions on Smart Grid, vol. 11, no. 3, pp. 2140 - 2150, May 2020

[30] 'Power quality aspects of solar power,' CIGRE working Group JWG C4/C6.29, Technical Brochure 672, Paris, France, Dec. 2016.

[31] G. Todeschini, S. Balasubramaniam, P. Igic, 'Time-Domain Modeling of a Distribution System to Predict Harmonic Interaction Between PV Converters,' IEEE Transactions on Sustainable Energy, vol. 10, no. 3, pp. 1450-1458, Feb. 22, 2019.

[32] S.A.U Islam, and D.S. Bernstein, 'Recursive Least Squares for Real-Time Implementation [Lecture Notes]'. IEEE Control Systems Magazine 39, no. 3, pp.82-85, 2019.

[33] O.S. Nduka, B.C. Pal. 'Harmonic characterisation model of grid interactive photovoltaic systems,' in 2016 IEEE International Conference on Power System Technology (POWERCON), pp. 1-6, Sept. 28, 2016.

[34] E. Abbasi, S. Shojae, P. Therrien, S. Rahman, J. Stangl, K. Strunz, S. Ahmad, 'Typical Canadian medium voltage benchmark network model for integration of distributed energy resources,' In Proc. CIGRE, pp. 1-8, Oct. 2016.

[35] R. Langella and A. Testa, 'IEEE standard definitions for the measurement of electric power quantities under sinusoidal, nonsinusoidal, balanced, or unbalanced conditions, 2010.

[36] A.E. Emanuel, 'Summary of IEEE standard 1459: definitions for the measurement of electric power quantities under sinusoidal, nonsinusoidal, balanced, or unbalanced conditions, IEEE transactions on industry applications, vol. 40, no. 3, pp. 869-876, May 2004

8 Appendix

8.1 Data description and preprocessing

Data acquired from the field measurements are recordings of the voltage and current waveforms with brief description as stated in Table 3. Indeed, as all

Table 3: Description of the data acquired from field measurement

Description	Value
Samples per cycle	256
Cycle per snapshot	6
Seconds for each snapshot	1

data-intensive techniques rely on the quality of dataset used in the analysis, it is obvious that care and rigorous steps must be taken at the data pre-processing stages. We have carefully addressed possibilities of noise in the data at the data mining stage through detection of outliers. This is in line with technical works in existing literature - [8].

8.2 Voltage THD calculation based on IEEE Standard 1459

From [35, 36], for a 4-wire unbalanced network with nonsinusoidal voltages, the equivalent voltage THD is computed as shown below.

$$\text{Effective Voltage} \quad V_{eff} = \sqrt{\frac{1}{18}\Big(3\big(V_a^2+V_b^2+V_c^2\big)+\big(V_{ab}^2+V_{bc}^2+V_{ca}^2\big)\Big)} \tag{45}$$

$$\text{Fundamental frequency effective voltage} \quad V_{eff,1} = \sqrt{\frac{1}{18}\Big(3\big(V_{a1}^2+V_{b1}^2+V_{c1}^2\big)+\big(V_{ab1}^2+V_{bc1}^2+V_{ca1}^2\big)\Big)} \tag{46}$$

$$\text{Non-fundamental frequency effective voltage} \quad V_{eff,H} = \sqrt{\frac{1}{18}\Big(3\big(V_{aH}^2+V_{bH}^2+V_{cH}^2\big)+\big(V_{abH}^2+V_{bcH}^2+V_{caH}^2\big)\Big)} \tag{47}$$

$$V_{eff,H} = \sqrt{V_{eff}^2 - V_{eff,1}^2} \tag{48}$$

The equivalent voltage total harmonic distortion expression is given as stated below.

$$\text{Equivalent voltage THD} = \frac{V_{eff,H}}{V_{eff,1}} \times 100\% \tag{49}$$

For a three-phase 3-wire system, the following equations are used.

$$\text{Effective Voltage} \quad V_{eff} = \sqrt{\frac{1}{9}\left(V_{ab}^2 + V_{bc}^2 + V_{ca}^2\right)} \tag{50}$$

$$V_{eff,1} = \sqrt{\frac{1}{9}\left(V_{ab1}^2 + V_{bc1}^2 + V_{ca1}^2\right)} \tag{51}$$

$$V_{eff,H} = \sqrt{\frac{1}{9}\left(V_{abH}^2 + V_{bcH}^2 + V_{caH}^2\right)} \tag{52}$$

Using the above expressions, the equivalent voltage THDs have been calculated for the first ten intervals for the different simulation scenarios considered in this technical work - see Tables 4 and 5. Table 6 shows the voltage THDs where the traditional method has rather been applied.

Table 4: PCC at LV: Calculated equivalent voltage THD (%) at node '9' based on IEEE standard 1459 - 2010 [35]

Interval	Radial configuration	Weakly-meshed
1	0.0074	0.0033
2	0.0018	0.0009
3	0.0011	0.0006
4	0.0012	0.0007
5	0.0264	0.0135
6	0.0042	0.0023
7	0.0019	0.0010
8	0.0010	0.0005
9	0.0007	0.0003
10	0.0003	0.0002

8.3 Additional plots

Below are additional (9^{th} and 11^{th} harmonic frequencies) plots realised from this study.

Table 5: PCC at HV: Calculated equivalent voltage THD (%) at node '9' based on IEEE standard 1459 - 2010 [35]

Interval	Radial configuration	Weakly-meshed
1	0.6646	0.3463
2	0.2310	0.1205
3	0.1496	0.0780
4	0.1571	0.0820
5	3.2371	1.6887
6	0.6052	0.3157
7	0.2150	0.1121
8	0.1050	0.0548
9	0.0719	0.0375
10	0.0403	0.0210

Table 6: Radial configuration: traditional voltage THD (%) at node '9'

Interval	Phase-A	Phase-B	Phase-C
1	0.9629	0.8718	0.9470
2	0.3322	0.1275	0.3274
3	0.2153	0.1395	0.2120
4	0.1882	0.1414	0.1856
5	4.1936	2.6550	4.1346
6	0.8866	0.2480	0.8738
7	0.3279	0.1338	0.3230
8	0.1252	0.0867	0.1235
9	0.1085	0.0281	0.1069
10	0.0528	0.0403	0.0520

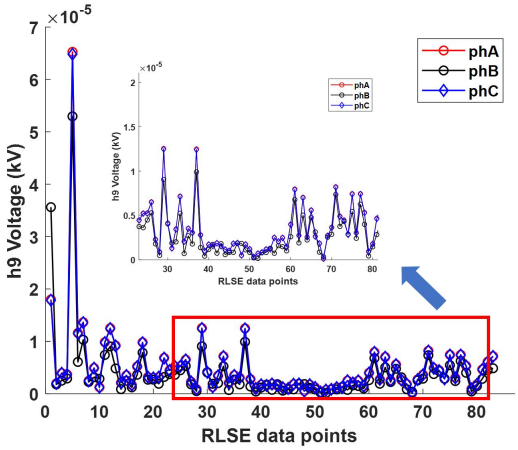

Figure 20: Meshed: ninth harmonic voltage when PCC is at the LV side

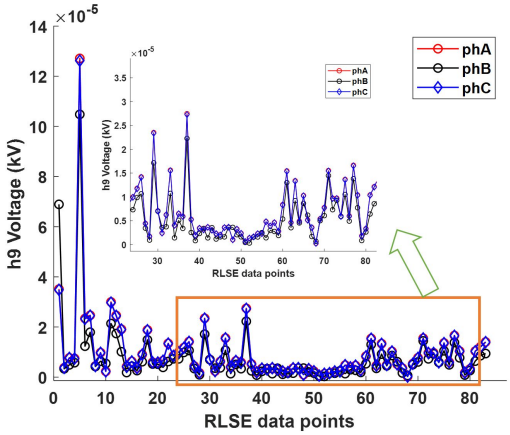

Figure 21: Radial: ninth harmonic voltage when PCC is at the LV side

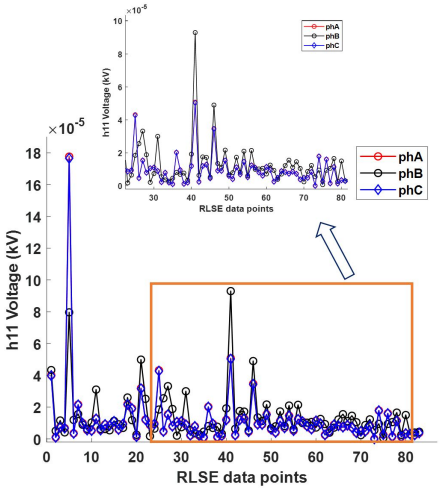

Figure 22: Radial: eleventh harmonic voltage when PCC is at the LV side